Desalination and Water Treatment
www.deswater.com
doi: 10.5004/dwt.2021.27058

221 (2021) 207–217
May

Kinetic models of competitive adsorption of cadmium–iron mixture on montmorillonite

Radhia Yous[a], Hakima Cherifi[a,*], Razika Khalladi[b]

[a]*Laboratoire des Biomatériaux et des Phénomènes de Transferts LBMPT, Université de Médéa, Médéa 26000, Algérie, emails: ha_cherifi@yahoo.fr (H. Cherifi), radia_yr@yahoo.fr (R. Yous)*
[b]*Laboratoire des Matériaux et Environnement LME, Université de Médéa, Médéa 26000, Algérie, email: r_khalladi@yahoo.fr*

Received 8 July 2020; Accepted 15 January 2021

ABSTRACT

In this work, montmorillonite (MNT) extracted from Algerian clay is used to remove cadmium and iron that are found simultaneously in wastewaters. The effects of pH, initial adsorbate concentration (C_0), and adsorbent concentration (C_B), on competitive adsorption of both metals were studied in batch system. MNT was analyzed by infrared, scanning electron microscopy with energy dispersive X-ray analysis, and Brunauer–Emmett–Teller. The kinetic models tested are: Boyd's, Weber and Morris external models, Urano and Tachikawa, Weber and Morris internal models, Elovich, pseudo-first and pseudo-second-order models. These models were compared based on: root mean square error, mean relative error deviation, mean absolute error, coefficient of correlation, accuracy, and bias factors. The competitive sorption of both metals is controlled by diffusion in pores and mésopores, and follows the Weber and Morris internal model. The statistical coefficients for this model are the most significant based on B_f values. Also, the estimated error coefficients show that kinetics of Cd and Fe fit well Elovich and pseudo-second-order models, respectively. The maximum uptakes are respectively 76 and 55 mg g^{-1} after 120 min. Raw MNT showed remarkable efficiency for the simultaneous sorption of cadmium and iron, especially for Cd. So, it could be suggested as a low cost adsorbent for effluents charged with cadmium.

Keywords: Kinetic mass transfer models; Competitive adsorption; Statistical error; Cadmium; Iron

1. Introduction

The presence of chemical products in industrial effluents causes water pollution. It degrades the quality of water and disrupts the aquatic environment [1]. These substances caused a serious public health problem [2]. Indeed, several compounds containing cadmium and iron are classified in the list of carcinogenic products. The presence of iron in the water at low concentrations can cause organ dysfunction and tissue damage in human bodies [3,4]. In addition, iron can act as a substrate for certain bacteria to cause health problems. In fact, studies have shown that iron can interact with microbial pathogens to increase their infectious potential, survivability, and stability [5,6]. Chronic exposure to cadmium, by inhalation or ingestion, results in kidney damage, bone damage even if absorption by ingestion is low, and chronic exposure to high levels of cadmium in food has caused bone disorders [7,8].

Among these heavy metals, cadmium and iron are used in many industries such as textiles, refineries, plastics, pigments, paints [9], battery storage, and petroleum [10]. In general, these two metals are not encountered separately but together as a mixture in the wastewater of these industries. Several compounds containing cadmium and iron are classified as carcinogens and can induce many types of

* Corresponding author.

cancer [11]. It is therefore essential to use efficient processes not expensive to treating this type of effluent industry.

Many methods and remediation techniques are developed to remove heavy metals. The adsorption on natural and abundant materials is a method of choice, effective, and economical to reduce the fraction of heavy metals in the wastewater of these industries [10,12]. The maximum concentrations of cadmium and iron in discharges of industrial liquid effluents are 0.2 and 3 mg L^{-1}, respectively [13].

The kinetics of adsorption is an important physicochemical parameter in the estimation of the qualities of a good sorbent. They describe the adsorption capacities, the time required for a particle to pass into a solid–liquid system, and the stages of the passage of the adsorbates to reach their sites.

The determination of the limiting step consists of finding the quantities adsorbed according to different models as a function of time. To do this, we have chosen to check the sorption mechanism that corresponds to the best conditions.

The main objective of this study is first, the valorization of a very abundant Algerian clay: montmorillonite (MNT) as a natural adsorbent [14,15]. Thus, competitive sorption of cadmium and iron ions on MNT was investigated to study the adsorption mechanism of these two metals. Secondly, the use of recent statistical models [16,17] such as the root mean square error (RMSE), mean relative error deviation (ARED), mean absolute error (MAE), and coefficient of determination (R^2) to describe the reliability of mathematical models. Moreover, the calculation of the precision (A_f) and bias (B_f) factors makes it possible to determine the global agreement between the values calculated by the theoretical models and the experimental values.

The mathematical models used are: Boyd external model, Weber and Morris external model, Urano and Tachikawa model, the internal diffusion of Weber and Morris model, pseudo-first-order and pseudo-second-order kinetic models, and Elovich model.

2. Materials and methods

2.1. Adsorbent and chemicals

The MNT used in this work is obtained from the bentonite extracted from the Hammam–Boughrara deposit in Maghnia (Tlemcen) that was provided by the company ENOF. Chemicals ($FeSO_4$ and $CdS0_{4,8/3H_2O}$) were used as provided. The stock solution was successively diluted with deionized water to obtain the desired concentration of metal. All the chemicals used in the study were of analytical reagent grade and all experiments were at room temperature.

2.2. Characterization

The composition of the MNT was determined by using several analysis methods, such as specific functional groups in the sorbent were identified using SHIMADZU 8400S Fourier transform infrared (FTIR) spectroscopy system (Shimadzu, Europe). The surface morphology of the MNT was examined using a scanning electron microscopy-energy dispersive X-ray spectroscopy (SEM/EDX) system (SEM/EDXQUANTA 650). Brunauer–Emmett–Teller (BET) surface area was analyzed by ASAP 2020 V3.04 H instrument.

2.3. Adsorption isotherm study

The competitive sorption of cadmium and iron ions from an aqueous solution was investigated by batch method. The ion concentrations remaining in the solution at equilibrium in the mixture were determined by UV spectrophotometer (UV-mini 1240 SHIMADZU) at a wavelength of 218 nm for cadmium and 312 nm for iron.

Adsorption capacity (q) and adsorption efficiency (E) were determined based on the Eqs. (1) and (2):

$$q = \left(\frac{C_0 - C}{m}\right)V \tag{1}$$

$$E\,(\%) = \left(\frac{C_0 - C}{C_0}\right)\cdot 100 \tag{2}$$

where C_0 (mg L^{-1}), C (mg L^{-1}) are, respectively, the initial concentration and the concentration at time t. The adsorbent concentration $C_B = m/V$, with m (g) and V (mL) are the mass of adsorbent and the volume of adsorbate, respectively.

The comparison between the kinetic models and the experimental data is based on the MAE, the RMSE and the ARED (%), the coefficient of determination (R^2), the precision (A_f), and bias (B_f) factors, Eqs. (3)–(8) describe all errors functions, respectively [18,19]:

$$\mathrm{MAE} = \frac{1}{N}\sum_{i=1}^{N}\left|q_{\exp} - q_{\mathrm{cal}}\right| \tag{3}$$

$$\mathrm{RMSE} = \sqrt{\frac{\sum\left(q_{\exp} - q_{\mathrm{cal}}\right)^2}{N}} \tag{4}$$

$$\mathrm{ARED} = \frac{1}{N}\sum\left(\frac{q_{\exp} - q_{\mathrm{cal}}}{q_{\exp}}\right)\cdot 100 \tag{5}$$

$$R^2 = 1 - \frac{\sum_{i=1}^{N}\left(q_i^{\exp} - q_i^{\mathrm{cal}}\right)^2}{\sum_{i=1}^{N}\left(q_i^{\exp} - \overline{q^{\exp}}\right)^2} \tag{6}$$

$$A_f = 10^{\left(\frac{\sum_{i=1}^{N}\left|\log\frac{q_i^{\mathrm{cal}}}{q_i^{\exp}}\right|}{N}\right)} \tag{7}$$

$$B_f = 10^{\left(\frac{\sum_{i=1}^{N}\left|\log\frac{q_i^{\mathrm{cal}}}{q_i^{\exp}}\right|}{N}\right)} \tag{8}$$

According to Soleiminie, the values of B_f make it possible to indicate the suitability and significance of a mathematical model. Values of B_f = 0.9–1.05 indicates that the model is good and correlates well with the experimental results, and the model is acceptable for B_f = 0.7–0.9.

Moreover, values of B_f between 1.06 and 1.15 show that the model could be used with prudence.

3. Results and discussion

3.1. Characterization of MNT

3.1.1. Structural characterization by infrared spectroscopy analysis

The FTIR spectral in Fig. 1 reveals the bands belonging to MNT before and after adsorption. The most intense groups are found at 1,033.88 cm^{-1} (stretching Si–O in the plane) and at 524.66 cm^{-1} (Si–O bending vibration). The distinct bands recorded at 524.66 and 470.65 cm^{-1}; are attributed, respectively, to the deformation vibrations Si–O–Al and Si–O–Mg. The wide bands at 3,441.12 and 1,643.41 cm^{-1} represent respectively the stretching and bending vibrations of the OH water molecules. Where bands between 1,600 and 1,700 cm^{-1} are attributed to the vibrations of the OH group originated from the water of constitution plus the binding vibrations of the water molecules adsorbed between the layers. The band located in the interval 3,200–3,800 cm^{-1}, with an intense peak at 3,626.29 and 3,433.41 cm^{-1} is a typical characteristic of smectite. The band at 3,626.29 cm^{-1} corresponds to the vibrations of elongation of OH groups – of the octahedral layer coordinated to 2 Al. The band detected at 786.98 cm^{-1} can be attributed to disordered tridymite [20]. After adsorption, few changes were detected in the IR spectra. The main bands presenting low intensity were detected with some deviation either positive or negative.

3.1.2. SEM and EDX analyses

The SEM images presented in Fig. 2 revealed the homogeneity of the MNT surface with many cavities and bumps. Fig. 2 showed a layered morphology characteristic for silicates materials. Prominent C, O, Mg, Si, Al, and O peaks from EDX spectra (Fig. 3) confirm our elemental analysis result. The EDX analysis also identifies the presence of potassium and Ca in the sample shown in Table 1. Table 1 indicates that the predominant clay mineral is composed of oxygen and silicium present frequently in MNT.

3.1.3. BET surface area report

Table 2 summarizes the structural properties of the MNT. These results confirm the mesoporous structure of this material having pore widths from 20 to 500 Å [21]. Also, a low microporous volume of 6.1 × 10^{-3} cm^3 g^{-1}, and a reasonable specific surface area of 46.68 m^2 g^{-1} were obtained for this raw material.

The difference between the areas and diameters from adsorption and desorption branches is well discussed by [22]. Indeed, the isotherm of the untreated MNT studied in this work presented a hysteresis loop. The pore size distribution is influenced by the shape of the pores (ink bottle, etc.). When the pressure is reduced, the liquid will evaporate from the large pores, but the pores with narrow channels remain filled, giving different values for the two branches.

3.1.4. Physicochemical properties of adsorbents

The results of the physicochemical characterization of MNT are collated in Table 3.

The pH at which the sum of the surface charges is zero is known pH of zero charge point (pH_{Zero}). Above this value, the surface charge of our sorbent would be negative so that both metals could be adsorbed by cation exchange. The contrast would be observed below this value.

3.2. Parametric study

Adsorption capacity (q) and adsorption efficiency (E) of the cadmium–iron mixture as a function of the different parameters were determined to find optimal conditions. The results are presented in Fig. 4. The value of the optimum concentration of adsorbent in the mixture is C_B = 1 g L^{-1}. At this value, the maximum adsorption capacities were

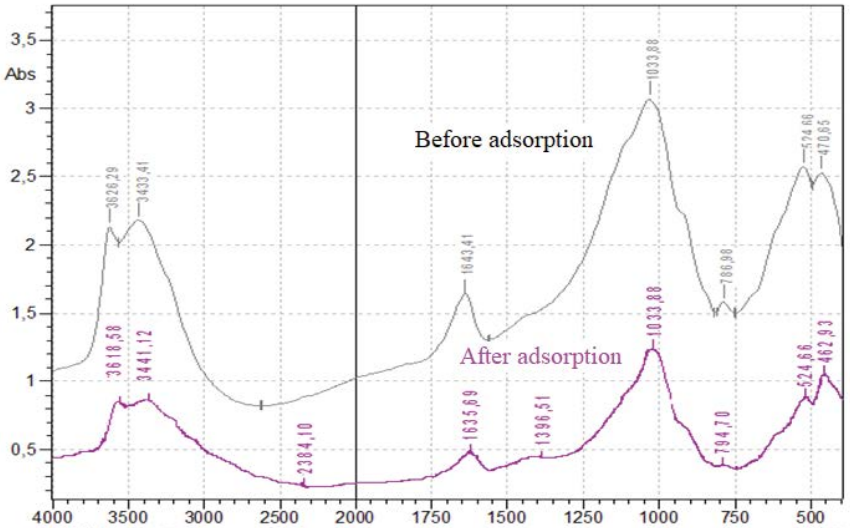

Fig. 1. Infrared spectrum of unloaded montmorillonite before and after sorption.

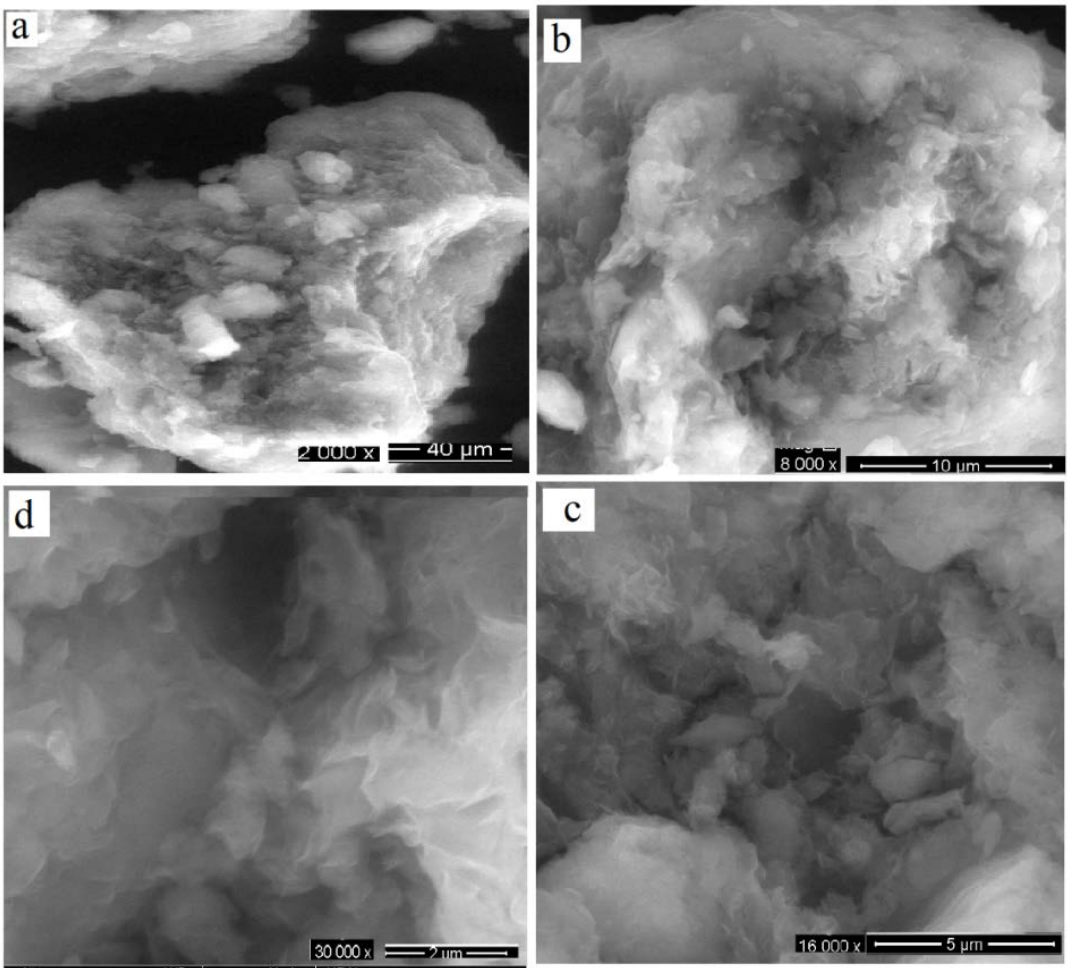

Fig. 2. SEM images of montmorillonite (a) 40 µm, (b) 10 µm, (c) 5 µm, and (d) 2 µm.

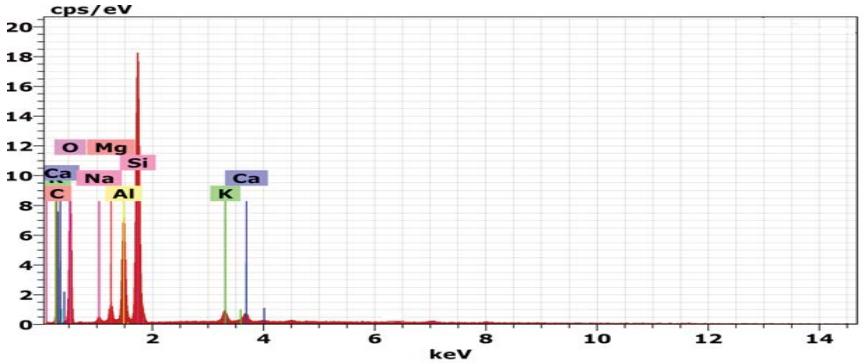

Fig. 3. EDX spectra of montmorillonite.

obtained for an initial concentration of 150 mg L^{-1} for each metal. The pH was tested at different values (4, 6, 8, 10, and 12). Based on the pH_{zero} value (Table 3), the MNT surface is negatively charged at pH ≥ 8. It was found that the adsorptions capacity rate is higher at pH equal to 10 for cadmium and 8 for iron. The difference observed between cadmium and iron, could be explained by the electronegativity values (1.69 for Cd and 1.83 for Fe). The presence of hydroxyl groups (Fig. 1) on the surface of the sorbent reflects the alkalinity of MNT.

3.3. Effect of contact time

The kinetic of the simultaneous adsorption of cadmium and iron on MNT was studied for different initial concentrations. At first, the initial concentration of iron was fixed

at 150 mg L^{-1} with a variable initial concentration of cadmium in the range C_{cd} = 50–300 mg L^{-1}. Fig. 5 represents the kinetics adsorption of cadmium.

Then, the initial concentration of cadmium was fixed (150 mg L^{-1}), and the concentration of iron is varied from 50 to 300 mg L^{-1}. The results are represented in Fig. 6.

As shown in Figs. 5 and 6, the quantity adsorbed increases with both metal initial concentrations, followed by a step corresponding to the saturation of the active sites of MNT. The equilibrium time for both metals is 2 h for the different initial concentrations.

3.4. Kinetic models

Fig. 7 represents the adsorption kinetic of cadmium–iron mixture on MNT under optimum conditions. The kinetics of both metals reveals that initially, the quantity adsorbed increases remarkably. After that, the quantity adsorbed increases slowly with time reaching approximately 76 mg Cd g^{-1} for cadmium. However, in the case of iron, the quantity adsorbed reached 55 mg Fe g^{-1}.

The envisaged mechanisms of the adsorption process could be as follows [23,24]:

- Mass transfer of the two metals to the surface of montmorillonite (in the film),
- Adsorption of the metal ion on the sites,
- Internal diffusion of the metal ion on montmorillonite.

In order to determine the kinetic model that describes with accuracy the competitive sorption of Cd–Fe on MNT. The following models have been tested: the pseudo-first and the pseudo-second-order models, Elovich model, diffusion in the film defined by the external model of Boyd and external model of Weber and Morris, the intraparticle diffusion model of Weber and Morris, Urano and Tachikawa model (Fig. S1). The best fit was estimated statistically in terms of coefficient of determination (R^2), the accuracy (A_f), and bias (B_f) factors, MAE, RMSE, and ARED. The results and the equations of all these models are grouped in Tables 4–6.

According to Table 4, the estimated R^2 values (0.92) and all other coefficients (lowest error coefficients) show that the Elovich model fits well the kinetic of cadmium competitive adsorption. In fact, the value of B_f is between 0.9 and 1.05, revealing that this model represents well the experimental results of cadmium [17].

However, in the case of iron, the calculated statistical values give a good agreement for the pseudo-second-order model. The calculated statistical values for this model are the most significant. Moreover, a value of B_f included in the validity interval according to Soleiminie [17], confirms the suitability of the pseudo-second-order model. These results prove that the surface of MNT is heterogeneous and exhibit different activation energies for chemisorption [25].

The values of the external mass transfer coefficient given by the specific surface area (β/S) and those of the effective diffusion coefficient (D_i) obtained from each model for the cadmium–iron mixture, are of the same magnitude (Table 5). On one hand, the values of R^2 for both metals show that the simultaneous adsorption is better

Table 1
Results of analysis by EDX

Element	Weight (%)	Atomic (%)
Carbon	10.68	16.16
Potassium	0.83	0.38
Calcium	0.64	0.29
Oxygen	52.58	59.74
Aluminum	8.94	6.03
Sodium	1.04	0.83
Silicium	23.24	15.04
Magnesium	2.06	1.54
Total	100.00	100.00

Table 2
Results of analysis by nitrogen adsorption on montmorillonite

Characteristics	Parameter	Values
Surface area (m^2 g^{-1})	BET surface area	46.68
	External surface area	32.19
	Micropore area	14.48
	BJH adsorption cumulative surface area of pores	30.63
	BJH desorption cumulative surface area of pores	61.58
Pore size (Å)	BJH adsorption average pore diameter (4 V/A)	112.05
	BJH desorption average pore diameter (4 V/A)	59.88
Volume (cm^3 g^{-1}) × 10^3	Micropore volume	6.10

Table 3
Results of physicochemical characterization of montmorillonite

Parameters	d_p (m)	ρ_{app} (g cm^{-3})	$\rho_{effective}$ (g cm^{-3})	pH	pH_{Zero}	S (m^2/m^3)
Values	2×10^{-6}	1.11	4.28	10.24	8	4,050

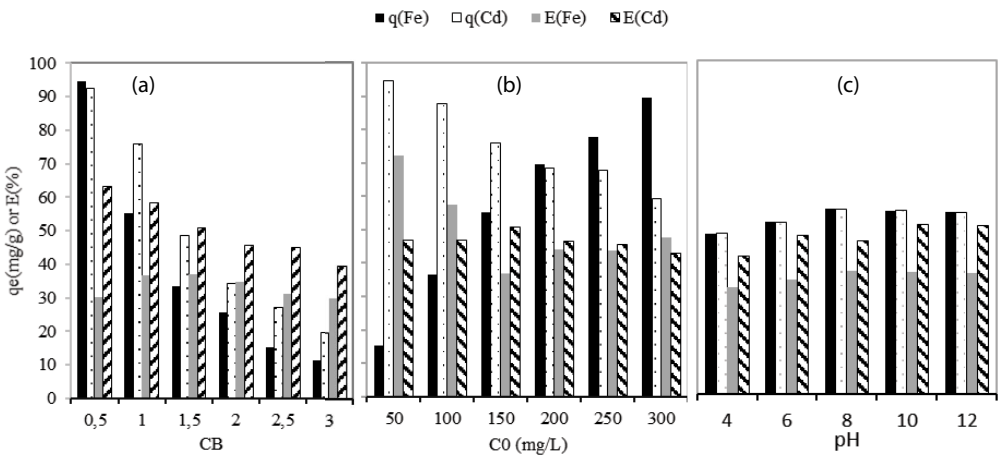

Fig. 4. Results of adsorption parametric study of cadmium–iron mixture on montmorillonite (T = 23°C). Effect of (a) adsorbate mass C_0 (Cd) = 150 mg L^{-1}, C_0 (Fe) = 150 mg L^{-1}, (b) initial concentration C_B = 1 g L^{-1}, and (c) initial pH of solution C_0 (Cd) = 150 mg L^{-1}, C_0 (Fe) = 150 mg L^{-1}, and C_B = 1 g L^{-1}.

Table 4
Parameters of pseudo-first and second-order and Elovich models for Cd/Fe

Models	Parameters	Cadmium	Iron	Equations		Ref.
Pseudo-first-order	K_1 (min^{-1})	0.004	0.009	$-\log_{10}\left[\frac{(q_e-q)}{q_e}\right]=\frac{K_1}{2.3}t$	(9)	[27]
	$q_{e,exp}$ (mg g^{-1})	76.002	55.325			
	$q_{e,cal}$ (mg g^{-1})	55.471	50.605			
	A_f	1.028	1.276			
	B_f	1.025	1.155			
	R^2	0.850	0.961			
	ARED	0.2624	0.544			
	RMSE	16.516	17.878			
	MAE	14.205	13.633			
Pseudo-second-order	K_2 (g mg^{-1} min^{-1})	0.0003	0.0022	$\frac{1}{q_e-q}=\frac{1}{q_e}-k_2t$	(10)	[28,29]
	$q_{e,exp}$ (mg g^{-1})	76.002	55.325			
	$q_{e,teo}$ (mg g^{-1})	73.136	53.605			
	A_f	1.533	1.023			
	B_f	0.579	0.978			
	R^2	0.910	0.98			
	ARED	1.151	0.07854			
	RMSE	86.686	4.692			
	MAE	60.625	1.793			
Elovich	a (g mg^{-1})	36.800	18.84	$q_t=\frac{1}{b}\ln(a\cdot b)+\frac{1}{b}\ln t$	(11)	[30,31]
	b (mg g^{-1} min^{-1})	0.220	0.209			
	A_f	1.0557	1.154			
	B_f	0.994	0.921			
	R^2	0.922	0.915			
	ARED	0.003	2.0972			
	RMSE	1.993	3.695			
	MAE	7.209	20.877			

represented by the Weber and Morris model. On the other hand, the statistical coefficients show that the adsorption of these metals is better represented by Boyd model. To resolve this contradiction, the Bias factor (B_f) values indicate that the Boyd model fits well the experimental results with values in the acceptable range.

Table 6 shows that the values of R^2 are so different for the two internal models. For both metals, the internal

model of Weber and Morris represents very well the experimental results in the three stages of adsorption. Indeed, the competitive sorption of these metals occurs mostly in the macropores and mesopores. Despite, the acceptable values of errors found for iron in the micropores step are acceptable, the mesoporous structure found by BET analysis confirm the heterogeneous nature of the MNT and that the simultaneous sorption of Cd and Fe occurs in the macropores and mesopores.

The values of the intraparticle diffusion coefficients (D_w, D_u) presented in Table 6 are almost of the same order as the external mass transfer coefficients given in Table 5. According to Yous et al. [26] for boundary diffusion to be a rate-limiting step, the value of the diffusion coefficient should be in the range 10^{-6}–10^{-8} cm^2 s^{-1}. Comparaison of Boyd model parameters with those of the internal model of Weber and Morris show that the internal diffusion in the macropores and mesopores is the controlling step of the competitive adsorption mechanism.

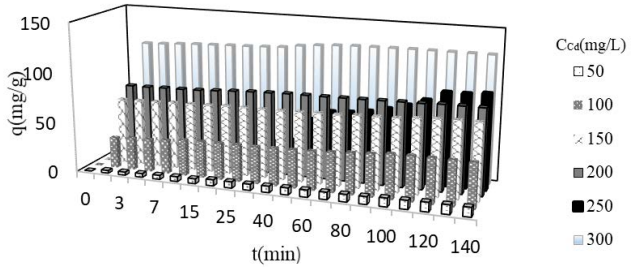

Fig. 5. Adsorption kinetics capacity for various initial cadmium concentrations, C_0 (Cd) = 150 mg L^{-1}, C_B = 1 g L^{-1}, and T = 23°C.

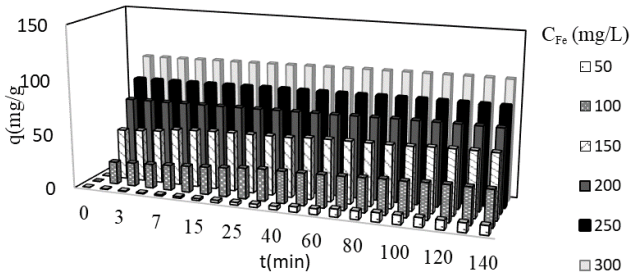

Fig. 6. Adsorption kinetics capacity for various initial iron concentrations, C_0 (Cd) = 150 mg L^{-1}, C_B = 1 g L^{-1}, and T = 23°C.

4. Conclusion

MNT extracted from Algerian clay is a source that is inexpensive and safe for the environment. In this work, the competitive sorption of cadmium and iron on this material seemed to be controlled by the diffusion in macrospores and mesopores. Based on R^2 and different error coefficients the Weber and Morris internal model is the most significant model that describes the sorption mechanism in the Cd–Fe mixture. Elovich and the pseudo-second-order models are found the most appropriate models that fit accurately the

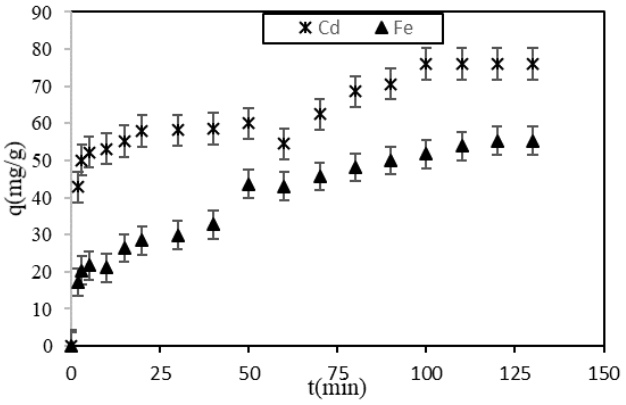

Fig. 7. Adsorption kinetics of cadmium–iron mixture on montmorillonite. C_0 (Cd) = 150 mg L^{-1}, C_0 (Fe) = 150 mg L^{-1}, C_B = 1 g L^{-1}, and T = 23°C.

Table 5
Parameters of Boyd, external Weber and Morris models for cadmium and iron

Models	Parameters	Cadmium	Iron	Equations		Ref.
Boyd	D_i (cm^2 s^{-1})	3.04×10^{-11}	2.03×10^{-11}	$B_t = -0.4977 - \log\left[1 - \frac{q}{q_e}\right]$	(12)	[32]
	A_f	1.048	1.18			
	B_f	1.019	1.16			
	R^2	0.806	0.798			
	ARED	0.044	0.231			
	RMSE	4.581	7.011			
	MAE	18.746	5.161			
Weber and Morris external	β (cm s^{-1})	4.90×10^{-9}	1.23×10^{-7}	$\frac{dq}{dt} = \beta A\left(C - C_s\right)$	(13)	[33,34]
	A_f	2.821	2.265			
	B_f	0.388	1.398			
	R^2	0.953	0.931			
	ARED	12.046	3.417			
	RMSE	5.861	2.717			
	MAE	35.408	6.836			

Table 6
Parameters of Weber and Morris internal and Urano and Tachikawa models for cadmium and iron

Models	Parameters	Cadmium	Iron	Equations		Ref.
Weber and Morris (macrospore)	D_W (cm² s⁻¹)	3.431×10^{-10}	4.363×10^{-11}			
	A_f	1.023	1.025			
	B_f	0.996	0.983			
	R^2	0.998	0.999			
	ARED	0.017	0.016			
	RMSE	1.068	2.586			
	MAE	1.189	0.504			
Weber and Morris (mesopore)	D_W (cm² s⁻¹)	2.099×10^{-11}	1.540×10^{-11}	$q = \left(\frac{12q_e}{d_p}\right)\left(\frac{D_W}{\pi}\right)^{0.5} t^{0.5} + I$	(14)	[35]
	A_f	1.012	1.025			
	B_f	1.012	1.006			
	R^2	0.929	0.905			
	ARED	0.843	0.003			
	RMSE	0.886	1.217			
	MAE	0.784	0.972			
Weber and Morris (macropore)	D_W (cm² s⁻¹)	11.102×10^{-11}	1.406×10^{-11}			
	A_f	1.064	1.028			
	B_f	1.073	0.982			
	R^2	0.957	0.998			
	ARED	5.544	0.016			
	RMSE	6.981	2.259			
	MAE	4.848	1.166			
Urano and Tachikawa (macrospore)	D_U (cm² s⁻¹)	4.6×10^{-11}	0.920×10^{-11}			
	A_f	1.029	0.858			
	B_f	1.029	1.164			
	R^2	0.771	0.851			
	ARED	0.074	0.121			
	RMSE	4.198	7.501			
	MAE	3.214	6.365			
Urano and Tachikawa (mesopore)	D_U (cm² s⁻¹)	0.690×10^{-12}	2.32×10^{-11}	$-\log_{10}\left[1-\left(\frac{q}{q_e}\right)^2\right] = \frac{4\pi^2 D_U t}{2.3 d_p^2}$	(15)	[36]
	A_f	1.112	0.067			
	B_f	0.927	1.636			
	R^2	0.804	0.792			
	ARED	0.0518	0.067			
	RMSE	10.904	1.636			
	MAE	4.031	1.384			
Urano and Tachikawa (micropore)	D_U (cm² s⁻¹)	6.900×10^{-11}	4.621×10^{-11}			
	A_f	1.135	0.963			
	B_f	0.882	1.085			
	R^2	0.989	0.877			
	ARED	0.0367	0.048			
	RMSE	11.172	1.708			
	MAE	0.671	1.416			

kinetics of cadmium and iron, respectively. Calculated values of the Bias factor were very useful when comparing the suitability of all tested models. The maximum adsorbed quantities of cadmium and iron are, respectively, 76 and 55 mg g^{-1} after 120 min for the following conditions: (C_0 = 150 mg L^{-1}), (C_B = 1 g L^{-1}), and pH = 10 for Cd and pH = 8 for Fe.

The present work shows that the use of MNT without any treatment as a natural low-cost sorbent is an economically and environmentally promising solution for the simultaneous removal of cadmium and iron from wastewater. Could be proposed, especially, for the treatment of effluents charged with cadmium.

Acknowledgments

The Algerian company of mineral and non-ferrous products, ENOF Maghnia (Algeria) is the source of bentonite, it facilitates the use of these adsorbents existing in very large quantities which makes authors thank this company for their support.

Symbols

a	—	Initial sorption rate, mg g^{-1} min^{-1}
A_f	—	Accuracy factor
ARED	—	Average relative error deviation
b	—	Extent of surface coverage, g mg^{-1}
B_t	—	Mathematical function of the value (q/q_e)
B	—	Slope of the linear part of the curve $B_t = f(t)$
B_f	—	Bias factor
C	—	Residual dye in solution, mg L^{-1}
C_B	—	Adsorbent concentration, g L^{-1}
C_e	—	Equilibrium adsorption concentration, mg L^{-1}
C_0	—	Initial adsorption concentration, mg L^{-1}
C_s	—	Adsorption concentration solute in the solid particle, g m^{-3}
d_p	—	Particle mean diameter, m
D_i	—	Effective diffusion coefficient in Boyd's model, cm^2 s^{-1}
D_u	—	Internal diffusion coefficient in Urano and Tachikawa model, cm^2 s^{-1}
D_w	—	Internal diffusion coefficient in Weber and Morris model, cm^2 s^{-1}
I	—	Intercept in Weber and Morris internal model
K_1	—	Rate constant of the pseudo-first-order adsorption, s^{-1}
K_2	—	Rate constant of pseudo-second-order adsorption, g mg^{-1} s^{-1}
MAE	—	Mean absolute error
pH	—	Potential hydrogen
pH_{Zero}	_	pH of zero charge point
q	—	Adsorption capacity, mg g^{-1}
q_{exp}	_	Experimental adsorption capacity, mg g^{-1}
q_{cal}	_	Calculated adsorption capacity, mg g^{-1}
R^2	—	Determination coefficient
RMSE	—	Root mean square error, %
S	—	Specific surface per unit volume of solution, m^2 m^{-3}
ρ_{app}	—	The apparent volumic mass, g cm^{-3}
ρ_{act}	—	Actual volumic mass, g cm^{-3}
β	—	External mass transfer coefficient, cm s^{-1}

References

[1] T. Chouchane, S. Chouchane, A. Boukari, A. Mesalhi, Adsorption of binary mixture Lead-Nickel by kaolin, J. Mater. Environ. Sci., 6 (2015) 924–941.
[2] S. Gu, X. Kang, L. Wang, E. Lichtfouse, C. Wang, Clay Mineral adsorbents for heavy metal removal from wastewater: a review, Environ. Chem. Lett., 17 (2019) 629–654.
[3] R. Yous, F. Mohellebi, H. Cherifi, A. Amrane, Competitive biosorption of heavy metals from aqueous solutions onto *Streptomyces rimosus*, Korean J. Chem. Eng., 35 (2018) 890–899.
[4] H. Fatima, A. Ambreen, Heavy metal pollution, J. Bacteriol. Mycol., 6 (2018) 179–181.
[5] G. Fongaro, A. Viancelli, D.A. dos Reis, A.F. Santiago, M. Hernández, W. Michellon, M.C. da Silva Lanna, H. Treichel, D. Rodríguez-Lázaro, Mineral waste containing high levels of iron from an environmental dis-aster (Bento Rodrigues, Mariana, Brazil) is associated with higher titers of enteric viruses, Food Environ. Virol., 11 (2019) 178–183.
[6] H.A. Aziz, H.A. Tajarudin, T.H.L. Wei, M.Y.D. Alazaiza, Iron and manganese removal from groundwater using limestone filter with iron-oxidized bacteria, Int. J. Environ. Sci. Technol., 17 (2020) 2667–2680.
[7] C.R. Johnson, J. Hopf, J.D. Shrout, J.B. Fein, Testing the component additivity approach to surface complexation modeling using a novel cadmium-specific fluorescent probe technique, J. Colloid Interface Sci., 534 (2019) 683–694.
[8] E.A.M. Yap, M. Mujawar, J. Sahu, Microwave induced synthesis of magnetic biochar from agricultural biomass for removal of lead and cadmium from wastewater, J. Ind. Eng. Chem., 45 (2017) 287–295.
[9] J. Zhang, H. Li, Y. Zhou, L. Dou, L. Cai, L. Mo, J. You, Bioavailability and soil-to-crop transfer of heavy metals in farmland soils: a case study in the Pearl River Delta, South China, Environ. Pollut., 235 (2018) 710–719.
[10] P.A. Kotabewatta, N. Priyantha, L.B.L. Lim, Biosorption of heavy metal ions on peel of *Artocarpus nobilis* fruit: 2. Improvement of biosorption capacities of Ni(II) through different modifications, Desal. Water Treat.,185 (2020) 226–236.
[11] E. Priya Rose, S. Rajam, Equilibrium study of the adsorption of iron(II) ions from aqueous solution on carbons from wild jack and jambul, Adv. Appl. Sci. Res., 3 (2012) 1889–1894.
[12] L.B.L. Lim, N. Priyantha, Y.C. Lu, N.A.H. Mohamad Zaidi, Adsorption of heavy metal lead using *Citrus grandis* (Pomelo) leaves as low-cost adsorbent, Desal. Water Treat., 166 (2019) 44–52.
[13] A. Ouyahia, Décret, Journal Officiel De La République Algérienne N°26, 2006.
[14] A.I. Vezentsev, D.M. Thuy, L.F. Goldovskaya-Peristaya, N.A. Glukhareva, Adsorption of methylene blue on the composite sorbent based on bentonite-like clay and hydroxyapatite, Indonesia J. Chem., 18 (2018) 733–741.
[15] H. Chen, L.K. Koopal, J. Xiong, M. Avena, W. Tan, Mechanisms of soil humic acid adsorption onto montmorillonite and kaolinite, J. Colloid Interface Sci., 504 (2017) 457–467.
[16] P.L. Mosquin, J. Aldworth, W. Chen, Evaluation of the use of bias factors with water monitoring data, Environ. Toxicol. Chem., 37 (2018) 1864–1876.
[17] R. Soleimani, A.H.S. Dehaghani, N.A. Shoushtari, P. Yaghoubi, A. Bahadori, Toward an intelligent approach for predicting surface tension of binary mixtures containing ionic liquids, Korean J. Chem. Eng., 35 (2018) 1556–1569.
[18] K. Amechi Ani, E.C. Chukwuma, Kinetics and statistical analysis of the bio stimulating effects of goat litter in crude oil biodegradation process, Beni-Suef Univ. J. Basic Appl. Sci., 29 (2020) 1–13.
[19] H. Cherifi, S. Hanini, F. Bentahar, Adsorption of phenol from wastewater using vegetal cords as a new adsorbent, Desalination, 244 (2009) 177–187.
[20] C. Paluszkiewicz, E. Stodolak, M. Hasika, M. Blazewicz, FT-IR study of montmorillonite–chitosan nanocomposite materials, Spectrochim. Acta, Part A, 79 (2011) 784–788.
[21] J. Rouquerol, D. Avnir, C.W. Fairbridge, D.H. Everett, J.M. Haynes, N. Pernicone, J.D.F. Ramsay, K.S.W. Sing, K.K. Unger, Recommendations for the characterization of porous solids (Technical Report), Pure Appl. Chem., 66 (1994) 1739–1758.
[22] F.D. Martijn, J.H.V. Thijs, G. Jorge, K. Freek, Adsorptive characterization of porous solids: error analysis guides the way, Microporous Mesoporous Mater., 200 (2014) 199–215.
[23] I. Ali, I. Burakova, E. Galunin, A. Burakov, E. Mkrtchyan, A. Melezhik, D. Kurnosov, A. Tkachev, V. Grachev, High-speed and high-capacity removal of methyl orange and malachite green in water using newly developed mesoporous carbon: kinetic and isotherm studies, ACS Omega, 4 (2019) 19293–19306.
[24] C.R. Girish, V. Ramachandra Murty, Mass transfer studies on adsorption of phenol from wastewater using *Lantana camara* forest waste, Int. J. Chem. Eng., 2016 (2016) 1–11.

[25] X. Liu, M. Zhou, X. Zhou, L. Wang, X. Liu, Functionalized poly(arylene ether nitrile) porous membrane with high Pb(II) adsorption performance, Polymers, 11 (2019) 1412–2019.
[26] R. Yous, H. Cherifi, R. Khalladi, Comparative mass transfer study of basic and acid magenta adsorption onto natural clay, Indonesia J. Chem., 19 (2019) 1031–1042.
[27] S. Lagergren, About the theory of so-called adsorption of soluble substances, Kungl. Svenska Vetenskapsakad. Handl., 24 (1898) 1–39.
[28] Y.S. Ho, G. MacKay, Pseudo-second-order model for sorption process, Process Biochem., 34 (1999) 451–465.
[29] Z. Aksu, Equilibrium and kinetics modelling of cadmium(II) biosorption by *C. vulgaris* in batch system: effect of temperature, Sep. Purif. Technol., 21 (2001) 285–294.
[30] Z. Wang, F. Yan, H. Pei, J. Li, Z. Cui, B. He, Antibacterial and environmentally chitosan/polyvinylalcohol blend membranes for air filtration, Carbohydr. Polym., 198 (2018) 241–248.
[31] T. Qian, N. Li, Q. Lu, X. Wang, Y. Zhu, Study on preparation and separation and adsorption performance of knitted tube composite - cyclodextrin/chitosan porous membrane, Polymers, 11 (2019) 1737, doi: 10.3390/polym11111737.
[32] G.E. Boyd, A.W. Adamson, L.S. Myers, The exchange adsorption of ions from aqueous solutions by organic Zeolites II. Kinetics, J. Am. Chem. Soc., 69 (1947) 2836–2848.
[33] G. MacKay, G. Poots, Kinetics and diffusion processes in colour removal from effluent using wood as an adsorbent, J. Chem. Technol. Biotechnol., 30 (1980) 279–292.
[34] G. MacKay, H.S. Blair, A. Fidon, Sorption of Metal Ions by Chitosan, In: Immobilisation of Ions by Biosorption, H. Eccles, S. Hunt, Eds., Ellis Horwood, UK, Chichester, 1986, pp. 59–69.
[35] J. Weber, C. Morris, Advances in water pollution research, Proc. Int. Conf. Water Pollut. Res., 162 (1992) 231–266.
[36] K. Urano, H. Tachikawa, Process development for removal and recovery of phosphorus from waste water by a new adsorbant, Ind. Eng. Chem. Res., 30 (1991) 1887–1899.

Supporting information

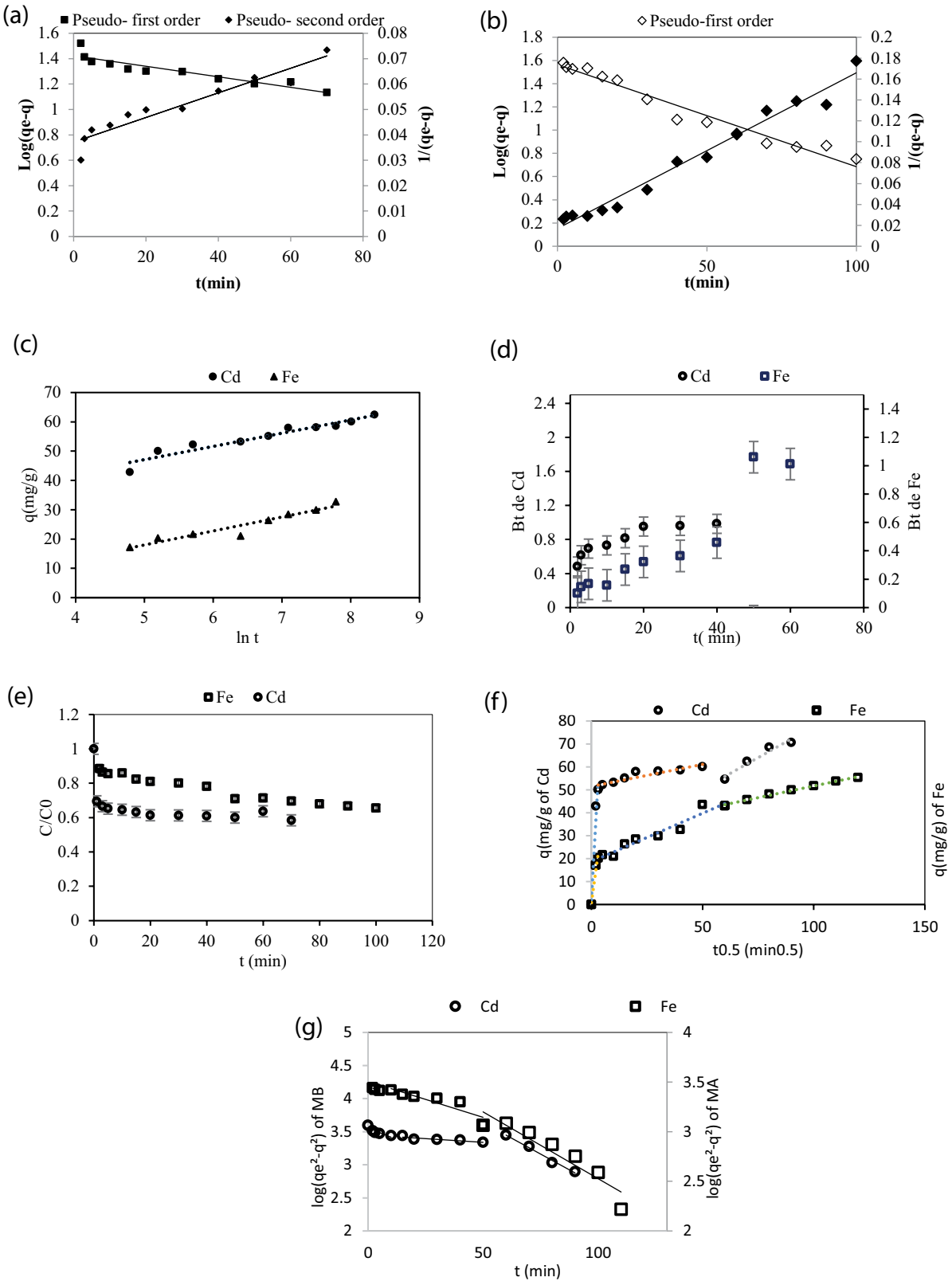

Fig. S1. Kinetic models of pseudo-first and second-order of (a) Cd, (b) Fe, (c) Elovich, (d) Boyd, (e) external Weber and Morris, (f) Weber and Morris internal, and (g) Urano and Tachikawa.